Springer

KSME

Journal of Mechanical Science and Technology 33 (8) (2019) 3895~3903
www.springerlink.com/content/1738-494x(Print)/1976-3824(Online)
DOI 10.1007/s12206-019-0733-z

Numerical analysis of the dynamic behavior of a rotor-bearing-brush seal system with bristle interference †

Yuan Wei and Shulin Liu*

School of Mechatronics Engineering and Automation, Shanghai University, Shanghai, 200444, China

(Manuscript Received February 21, 2019; Revised May 5, 2019; Accepted May 14, 2019)

Abstract

To minimize leakage and maintain the efficiency of turbomachinery, brush seal can be installed with zero clearance or interference as the flexibility. This leads to contact between the rotor and bristle pack, and may cause self-excited vibration, even instability. In this study, to establishment a mathematical model of the rotor system, a seal force model with bristle interference is proposed and the nonlinear oil-film force is applied in view of short bearing assumption. The influences of main factors containing rotor rotational speed, installing interval, disc mass, and disk eccentricity on the nonlinear characteristics of the rotor-bearing-brush seal system are conducted by adopting bifurcation diagram, spectrum cascade, axis orbit, and Poincaré map. The results indicate that the vibration amplitude of the system with bristle interference is a bit larger than that without interference. The system stability is enhanced with smaller disk mass at a higher rotational speed. The proposed model could provide valuable reference for the design of a rotor-bearing-seal system.

Keywords: Brush seal; Bristle interference; Seal force; Nonlinear dynamics

1. Introduction

Due to lower leakage, lighter weight, and longer service life, brush seals could enhance the working efficiency and reliability of turbomachinery [1, 2]. As a type of flexible contact seal, brush seals have many advantages over traditional labyrinth seal [3]. Labyrinth seal usually needs to set a radial clearance to avoid collision with the rotor, but the clearance in brush seal can be zero or even interference. It leads to acting force between the rotor and brush seal, and this may cause self-excited vibration and instability. So the development of a mathematical model for analyzing the rotor dynamic characteristics of rotor-bearing-brush seal system is of great importance to the stable operation of rotating machinery.

It is hard to estimate the contact force of brush seal due to the elastic deformation of bristles. Flower [4] adopted a simple cantilever beam formula to calculate the bristle tip force. Long and Marras [5] used a non-rotating experimental device for the force measurement of brush seal. But the predicted theoretical and experimental results were not exact enough, as the authors claimed themselves. Sharatchandra and Rhode [6] analyzed the bristle force under the undeflected condition. Zhao and Stango [7] developed a mechanic model to evaluate the contact force of single bristle with interference and fluid force. Demiroglu et al. [8] proposed an empirical model of seal tip force based on kinds of test results.

Until now, an abundant amount of work has been done and focused on the nonlinear behavior of a rotor system with consideration of the influence of nonlinear seal force and oil-film force [9-11], but most of the researches are focused on labyrinth seal using Muszynska model. The nonlinear performance analysis of rotor-bearing-brush seal system is still hardly known as lack of corresponding theory model for brush seal. In the present work, a nonlinear seal force model with bristle interference and eccentricity was established. The nonlinear oil-film force model with short bearing assumption was applied. The influence of rotational speed, installing interval, disk mass, and disk eccentricity on the dynamic characteristics of rotor system were presented.

2. Mathematical model of a rotor system

To investigate the seal force of brush seals and nonlinear behavior, lateral deflection of the disk is not considered here. Fig. 1 depicts the structural diagram of a rotor system.

2.1 Equations of motion

The dynamic equation of the 4-DOF rotor system could be derived as:

$$M\ddot{Q} + C\dot{Q} + KQ = -F_{\mathrm{g}} + F_{\mathrm{b}} + F_{\mathrm{s}} + F_{e}, \tag{1}$$

*Corresponding author. Tel.: +86 21 66130762
E-mail address: lsl346@shu.edu.cn
† Recommended by Associate Editor Junhong Park

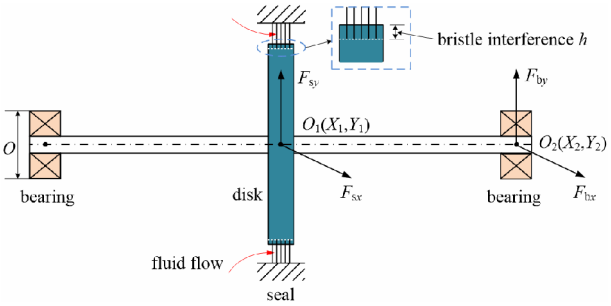

Fig. 1. Structure diagram of a rotor-bearing-brush seal system.

where M is the mass matrix of the system, $M=\begin{pmatrix} M_x & 0 \\ 0 & M_y \end{pmatrix}$, $M_x=M_y=\mathrm{diag}[M_\mathrm{d},M_\mathrm{b}]$, M_d and M_b are the mass of disk and bearing, respectively. C is the system damping matrix, $C=\begin{pmatrix} C_x & 0 \\ 0 & C_y \end{pmatrix}$, $C_x=C_y=\mathrm{diag}[C_1,C_2]$, C_1 and C_2 are the damping of disk and bearing, respectively. K is the rotor stiffness matrix, $K=\mathrm{diag}[K,K/2,K,K/2]$, Q are the displacements vectors of geometry center O_1 and O_2 in the X and Y directions, respectively, $Q=[X_1-X_2,X_2-X_1,Y_1-Y_2,Y_2-Y_1]^T$, F_g is the gravity vector of the rotor system, $F_\mathrm{g}=[0,0,M_\mathrm{d}g,M_\mathrm{b}g]^T$, F_b is the bearing oil-film force vector, $F_\mathrm{b}=[0,F_{\mathrm{bx}},0,F_{\mathrm{by}}]^T$, F_s is the seal force vector, $F_\mathrm{s}=[F_{\mathrm{sx}},0,F_{\mathrm{sy}},0]^T$, F_e is the unbalanced force vector, $F_e=[M_\mathrm{d}r_\mathrm{d}\omega^2\cos(\omega t),0,M_\mathrm{d}r_\mathrm{d}\omega^2\sin(\omega t),0]^T$, r_d is the eccentricity of disk.

2.2 Nonlinear seal force

To maintain sealing performance, the bristle tip is generally installed with an angle θ on the rotor. As the bristle is elastic, the radial interference of the bristle is an inevitable and significant phenomenon. Bristle interference is a kind of interference fit, which would affect the acting force between the rotor and bristle pack. It is assumed that the fluid flow is evenly distributed along a single bristle and the flow induced load in the axial direction is ignored. Fig. 2 depicts the force distributing diagrammatic sketch between rotor and bristle, and the bristle is treated as a cantilever beam.

As can be seen from Fig. 2(b), for a single bristle AB, bending deformation is mainly induced by flow force and rotor acting force. And the influence of shear stress is neglected as the length of bristle is much greater than the diameter of bristle. Then the expression of bristle bending can be obtained by using Euler-Bernoulli equation:

$$EI\frac{\mathrm{d}\varphi}{\mathrm{d}s}=M_F+M_q\,. \tag{2}$$

Through deduction of the bending moments induced by

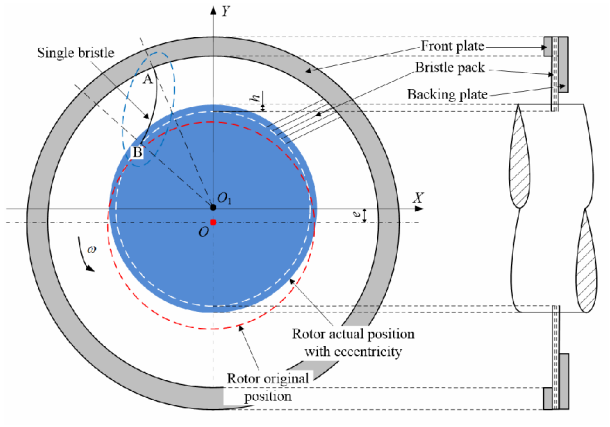

(a) Rotor and bristle contact schematic drawing

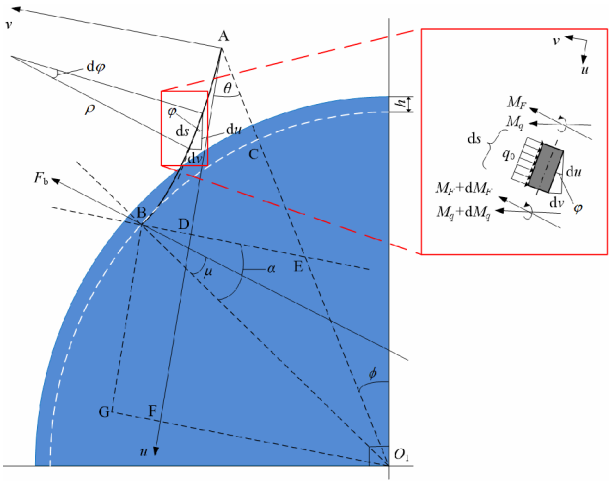

(b) Bending analysis of bristle with interference

Fig. 2. Force distributing diagrammatic sketch between the rotor and bristle.

contacting force F_b and uniformly distributed load of fluid flow q_0, Eq. (2) then can be rewritten as:

$$EI\frac{\mathrm{d}^2\varphi}{\mathrm{d}s^2}=-F_\mathrm{b}\sin(\alpha-\mu+\varphi)+q_0(L_1-s)\sin(\theta+\varphi)\,. \tag{3}$$

The value of bristle deflection Δv induced by F_b and q_0 at contact point B can be derived by superposition method:

$$\Delta v=\frac{F_\mathrm{b}L_1^3}{3EI}\cos(\alpha-\mu)-\frac{q_0L_1^4}{8EI}\sin\theta \tag{4}$$

with

$$L_1=AD=(R_\mathrm{b}+h-e\cos\phi-\frac{e^2}{2R}\sin^2\phi)\cos\theta-(R-h)\sin\alpha\,.$$

As observed in the right-angled trapezoid O_1GBE,

$$BD=(R-h)\cos\alpha-(R_\mathrm{b}+h-e\cos\phi-\frac{e^2}{2R}\sin^2\phi)\sin\theta\,. \tag{5}$$

Obviously, $\Delta v = BD$, so the expression of F_b can be obtained by solving Eqs. (4) and (5):

$$F_b = [(R-h)\cos\alpha - (R_b + h - e\cos\phi - \frac{e^2}{2R}\sin^2\phi)\sin\theta + \frac{q_0 L_1^4}{8EI}\sin\theta]\frac{3EI}{L_1^3\cos(\alpha-\mu)}. \quad (6)$$

It is assumed that all bristles are very tightly arranged in the bristle pack. As F_b is the contact force of a single bristle with an arbitrary position angle Φ, then the seal force in the x and y directions could be integrated by following expression [12]:

$$F_{sx} = \int_0^{2\pi} F_b \cos(\alpha - \mu + \theta - \phi)\mathrm{d}\phi, \quad (7)$$

$$F_{sy} = \int_0^{2\pi} F_b \sin(\alpha - \mu + \theta - \phi)\mathrm{d}\phi. \quad (8)$$

2.3 Nonlinear oil-film force

The expressions of oil-film force of bearing in the x and y directions could be deduced as follows by adopting the hypothesis of short bearing theory [13, 14]:

$$\begin{bmatrix} F_{bx} \\ F_{by} \end{bmatrix} = S_0 \begin{bmatrix} f_{bx} \\ f_{by} \end{bmatrix}. \quad (9)$$

The dimensionless oil-film force could be transformed as:

$$\begin{bmatrix} f_{bx} \\ f_{by} \end{bmatrix} = -\frac{\left[\left(x_2 - 2\dot{y}_2\right)^2 + \left(y_2 + 2\dot{x}_2\right)^2\right]^{1/2}}{1 - x_2^2 - y_2^2} \times \begin{bmatrix} 3x_2 V(x_2, y_2, \alpha) - G(x_2, y_2, \alpha)\sin\alpha - 2\cos\alpha S(x_2, y_2, \alpha) \\ 3y_2 V(x_2, y_2, \alpha) + G(x_2, y_2, \alpha)\cos\alpha - 2\sin\alpha S(x_2, y_2, \alpha) \end{bmatrix} \quad (10)$$

where

$$\alpha = \arctan\frac{y_2 + 2\dot{x}_2}{x_2 - 2\dot{y}_2} - \frac{\pi}{2}\mathrm{sign}\left(\frac{y_2 + 2\dot{x}_2}{x_2 - 2\dot{y}_2}\right) - \frac{\pi}{2}\mathrm{sign}\left(y_2 + 2\dot{x}_2\right) \quad (11)$$

$$G(x_2, y_2, \alpha) = \frac{2}{\left(1 - x_2^2 - y_2^2\right)^{1/2}}\left[\frac{\pi}{2} + \arctan\frac{y_2\cos\alpha - x_2\sin\alpha}{\left(1 - x_2^2 - y_2^2\right)^{1/2}}\right] \quad (12)$$

$$V(x_2, y_2, \alpha) = \frac{2 + \left(y_2\cos\alpha - x_2\sin\alpha\right)G(x_2, y_2, \alpha)}{1 - x_2^2 - y_2^2} \quad (13)$$

$$S(x_2, y_2, \alpha) = \frac{x_2\cos\alpha + y_2\sin\alpha}{1 - \left(x_2\cos\alpha + y_2\sin\alpha\right)^2}. \quad (14)$$

For easier calculation and derivation, dimensionless transformations are adopted:

Table 1. Structure and operating parameters of the rotor system.

Parameters	Value
E (Pa)	2.07×10^{11}
I (m^4)	1.278×10^{-18}
θ (°)	45
M_d (kg)	70
M_b (kg)	38
μ_0 (Pa.s)	0.2
r_d (m)	0.0005
δ_1 (m)	0.0004
δ_2 (m)	0.0002
R_2 (m)	0.03

$X_i = \frac{x_i}{\delta_i}$, $Y_i = \frac{y_i}{\delta_i}$, $q = [\frac{X_1}{\delta_1} - \frac{X_2}{\delta_2}, \frac{X_2}{\delta_2} - \frac{X_1}{\delta_1}, \frac{Y_1}{\delta_1} - \frac{Y_2}{\delta_2}, \frac{Y_2}{\delta_2} - \frac{Y_1}{\delta_1}]^T$, $\omega t = \tau$, $\frac{\mathrm{d}}{\mathrm{d}\tau} = \frac{\mathrm{d}}{\omega \mathrm{d}t}$, $\frac{\mathrm{d}^2}{\mathrm{d}^2\tau} = \frac{\mathrm{d}^2}{\omega^2\mathrm{d}t^2}$, where δ_1 is the moving range of the rotor, δ_2 is the bearing radial clearance, $S_0 = \mu_0\omega R_2 L_2(\frac{R_2}{\delta_2})^2(\frac{L_2}{2R_2})^2$, μ_0 is the absolute viscosity of lubricate, ω is the rotor rotational speed.

Then, Eq. (1) can be transformed as:

$$\omega^2\delta_j M\ddot{q} + \omega\delta_j C\dot{q} + Kq = -f_g + f_b + f_s + f_e \quad (i, j = 1, 2). \quad (15)$$

3. Numerical analysis and discussion

Numerical integration method is used to integrate Eq. (15). For describing the nonlinear dynamic responses of the rotor system, a bifurcation diagram, spectrum cascade, axis orbit, and Poincaré map are employed. Bifurcation occurs depending on the bifurcation parameter γ; when γ varies from the state branches to another state at a critical value γ_0, the dynamic behavior of the rotor system will change the motion states from stable to unstable. Power spectrum shows the frequency content of the time variation of the dynamical variables and helps to identify quasi-periodic and chaos motion. Axis orbit and Poincaré map can also valuably define the behavior of a system [15]. If the axis orbit is a regular circle and there exist n points in the Poincaré map, the system is in periodic-n motion or quasi-periodic motion. If the axis orbit is irregular and Poincaré map is discrete points, the system is in chaotic motion.

Table 1 lists the structure and operating parameters of the rotor system.

3.1 Effect of the rotor rotational speeds

Rotational speed is a main factor predicting the nonlinear behavior of a rotor system. Fig. 3 exhibits the bifurcation diagram and spectrum cascade of the system adopting rotor rotational speed as the controlling parameter; the rotational speed varies from 0 to 1200 rad/s. As can be seen from Fig. 3,

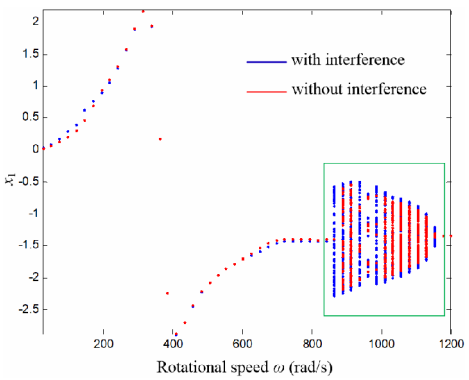

(a) Bifurcation diagram

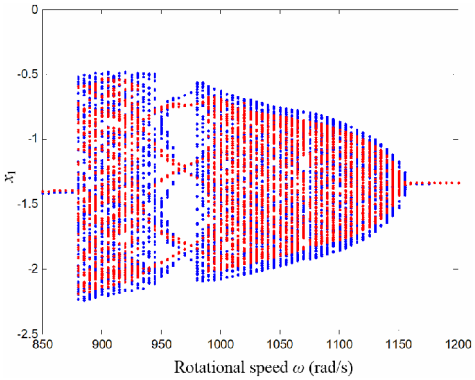

(b) Partially magnified bifurcation diagram

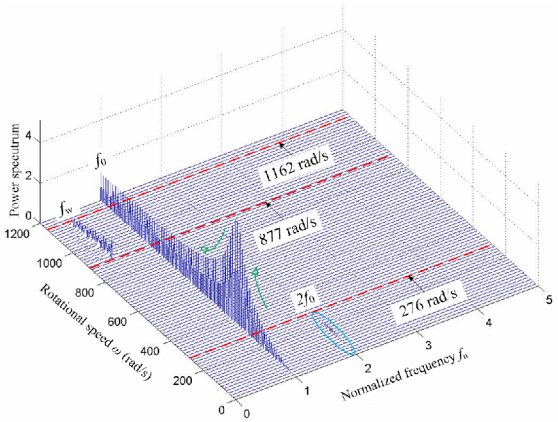

(c) Spectrum cascade with interference

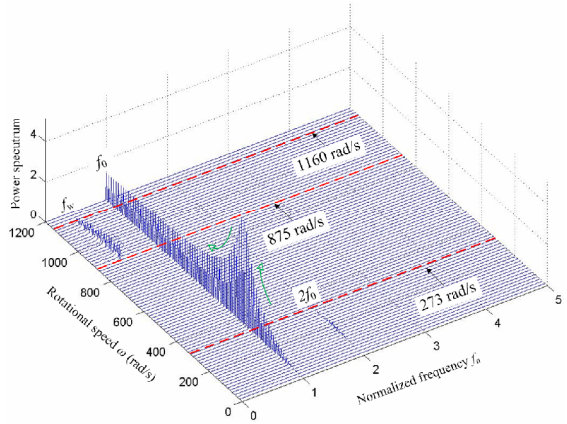

(d) Spectrum cascade without interference

Fig. 3. Bifurcation diagram and spectrum cascade with varying rotational speed.

the change trend of the system in the situation with and without bristle interference is roughly identical, but the vibration amplitude with interference is a bit larger than that without interference. The motion of the system with interference can be concluded as: Period-1 motion ($0 < \omega \leq 877$ rad/s) → quasi-periodic motion ($877 < \omega \leq 964$ rad/s) → period-5 motion ($964 < \omega \leq 979$ rad/s) → quasi-periodic motion ($979 < \omega \leq 1162$ rad/s) → period-1 motion ($1162 < \omega \leq 1200$ rad/s). And the system motion without bristle interference is: Period-1 motion ($0 < \omega \leq 875$ rad/s) → quasi-periodic motion ($875 < \omega \leq 934$ rad/s) → period-5 motion ($934 < \omega \leq 987$ rad/s) → quasi-periodic motion ($987 < \omega \leq 1160$ rad/s) → period-1 motion ($1160 < \omega \leq 1200$ rad/s). As plotted in Fig. 3(c), in the situation of with interference some small frequency components two-times of fundamental frequency $2f_0$ appear in the interval $\omega \in [0,276]$ rad/s. When $\omega \in [877,1162]$ rad/s, there are some frequency components f_w induced by self-excited synchronous vibration. And in the rest rotational speed the fundamental frequency f_0 dominates the spectrum. As illustrated in Fig. 3(d), without considering the bristle interference, the rotational speed intervals of appearing frequency components f_w and $2f_0$ decrease to $\omega \in [875,1160]$ rad/s and $\omega \in [0,273]$ rad/s, respectively.

For better understanding the vibration response of the rotor-bearing-seal system with and without bristle interference at different rotational speed, the axis orbits and Poincaré maps of the rotor system are presented in Fig. 4. When the rotational speeds are 410, 600, and 1200 rad/s, the rotor axis orbits are regular ellipses and the Poincaré maps are single points, which represent that the system is stable and in synchronous period-1 motion. When ω = 970 rad/s, rotor axis is irregular ring and five single points arise in Poincaré map, which illustrates that the system is in period-5 motion. And the axis orbit forms a sectorial ring and the Poincaré map forms one closed circle at ω = 1100 rad/s, which represents it is unstable and in quasi-periodic motion.

3.2 Effect of the installing interval

As bristle interference is the main focus in this paper, so the interference is considered in the following discussion. The operation range of a bristle pack is directly decided by the installing interval between the front plate and rotor surface. Bifurcation diagram and spectrum cascade varied by installing interval are shown in Figs. 5 and 6. From Fig. 5, it is clear the bifurcation diagram is a smooth upward line, illustrating that it is in period-1 motion. And there is only an f_0 in the spectrum cascade. As observed in Fig. 6, the bifurcation diagram is always in quasi-periodic motion when ω = 1000 rad/s, and combination of frequency components of f_w and f_0 appear-

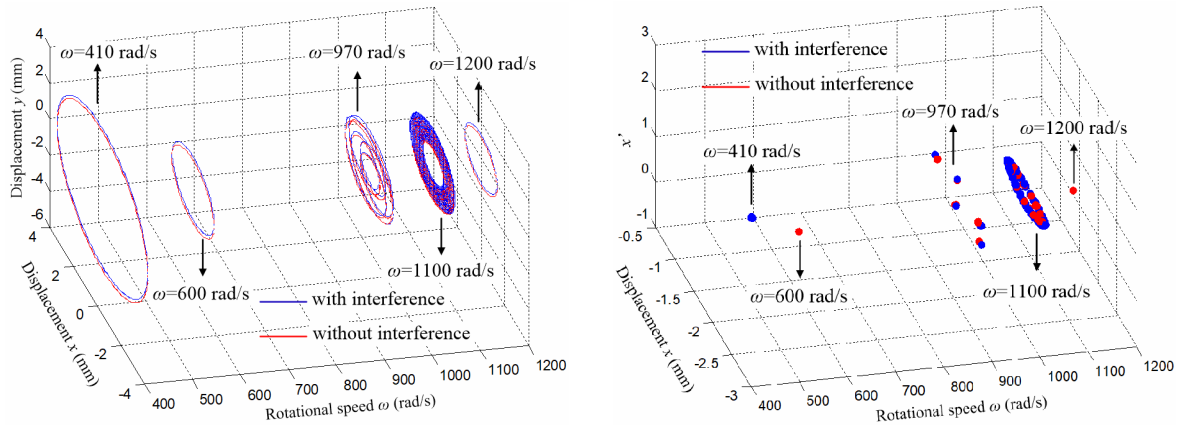

(a) Axis orbit (b) Poincaré map

Fig. 4. Vibration response at different rotational speed with interference and without interference.

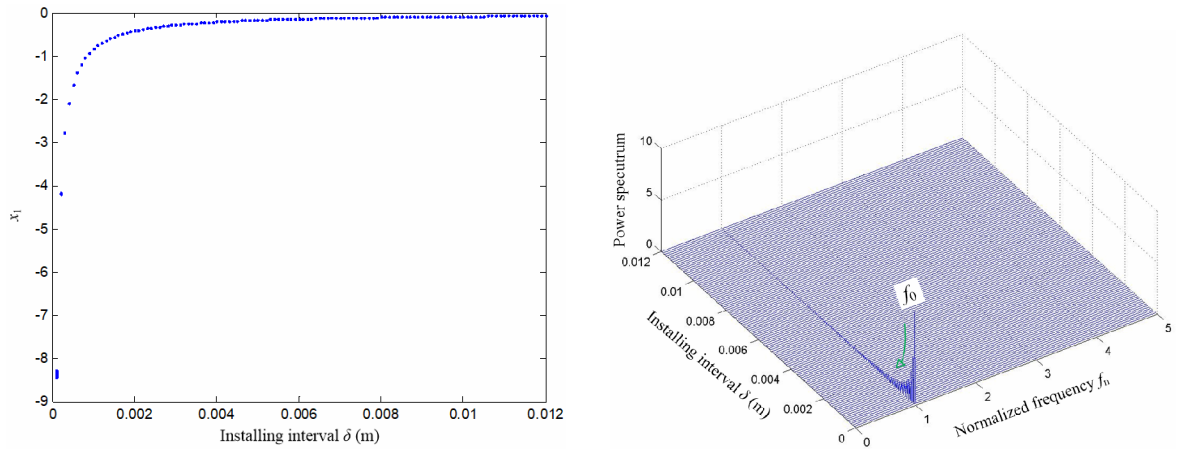

(a) Bifurcation diagram (b) Spectrum cascade

Fig. 5. Bifurcation diagram and spectrum cascade with varying installing interval at ω = 500 rad/s.

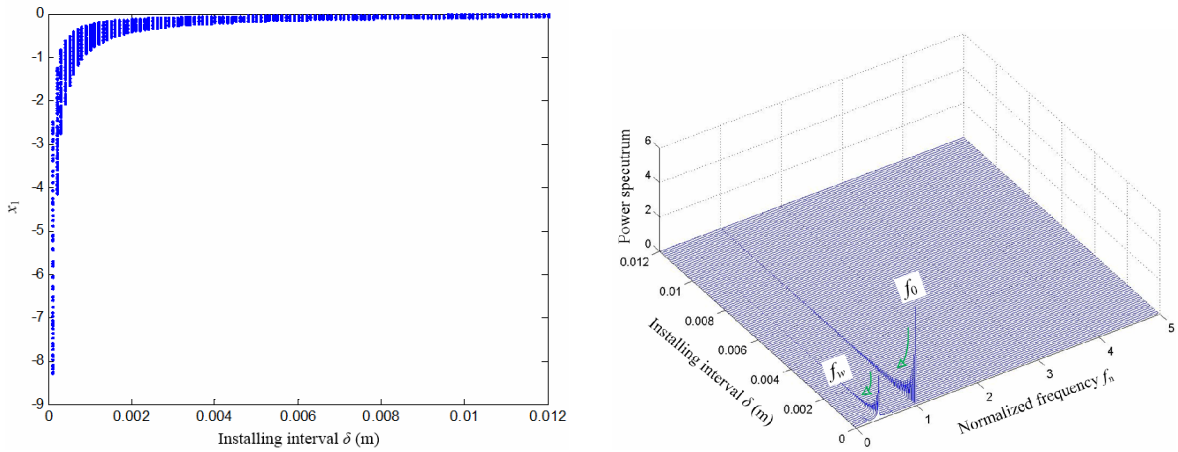

(a) Bifurcation diagram (b) Spectrum cascade

Fig. 6. Bifurcation diagram and spectrum cascade with varying installing interval at ω = 1000 rad/s.

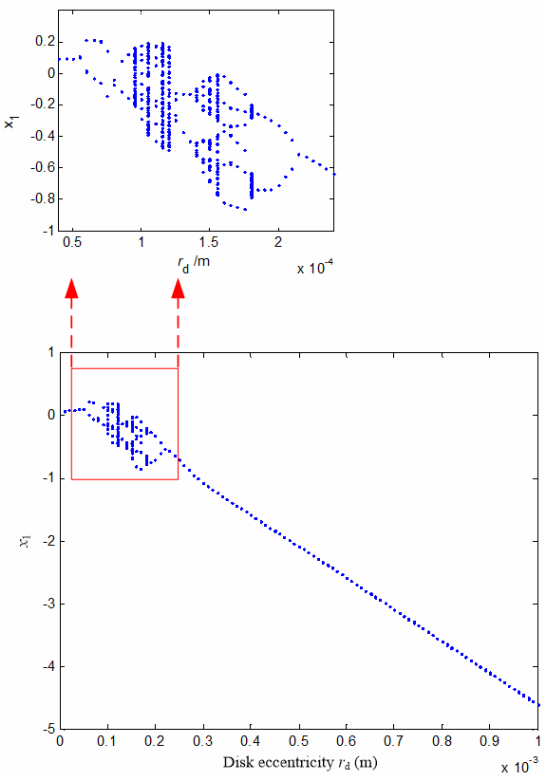

(a) Bifurcation diagram

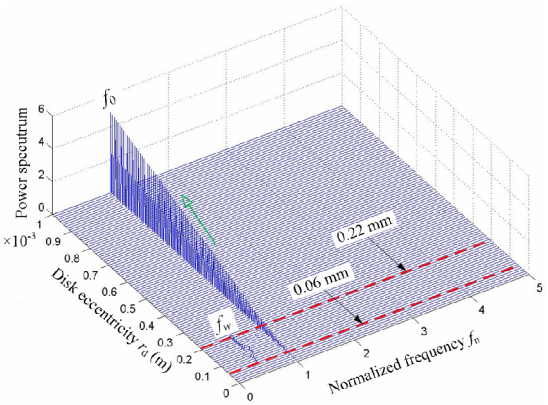

(b) Spectrum cascade

Fig. 7. Bifurcation diagram and spectrum cascade with varying disk eccentricity at ω = 500 rad/s.

ances through all value of installing interval variation. And the vibration amplitude decreases sharply at lower installing interval.

3.3 Effect of the disk eccentricity

An unbalanced mass could cause excited force and affect the system stability and dynamic performance. The bifurcation diagram and spectrum cascade by increasing disk eccentricity are shown in Figs. 7 and 8. As observed in Fig. 7(a), the motion of the system at $\omega = 500$ rad/s undergoes the following: Period-1 motion ($0 < r_d \le 0.06$ mm) → period-2 motion ($0.06 < r_d \le 0.09$ mm) → quasi-periodic motion ($0.09 < r_d \le 0.12$ mm) → period-2 motion ($0.12 < r_d \le 0.14$ mm) → quasi-periodic motion ($0.14 < r_d \le 0.16$ mm) → period-6 motion ($0.16 < r_d \le 0.18$ mm) → period-2 motion ($0.18 < r_d \le 0.22$ mm) → period-1 motion ($0.22 < r_d \le 1$ mm). There exist combination frequency components of f_w and f_0 when $r_d \in$ [0.06,0.22] mm, and the value of fundamental f_0 increases the disk eccentricity r_d (see Fig. 7(b)). As illustrated in Fig. 8(a), the motion at ω=1000 rad/s can be concluded as: Period-1 motion ($0 < r_d \le 0.26$ mm) → quasi-periodic motion ($0.26 < r_d \le 0.40$ mm) → period-5 motion ($0.40 < r_d \le 0.44$ mm) → quasi-periodic motion ($0.44 < r_d \le 0.69$ mm) → period-1 motion ($0.69 < r_d \le 1$ mm). As shown in Fig. 8(b), f_w appears at 0.26 mm and disappears at 0.69 mm. The axis orbit and Poincaré map in Fig. 9 can further illustrate the changing process from synchronous motion to oil whirl, and reach a stable state with the increase of r_d.

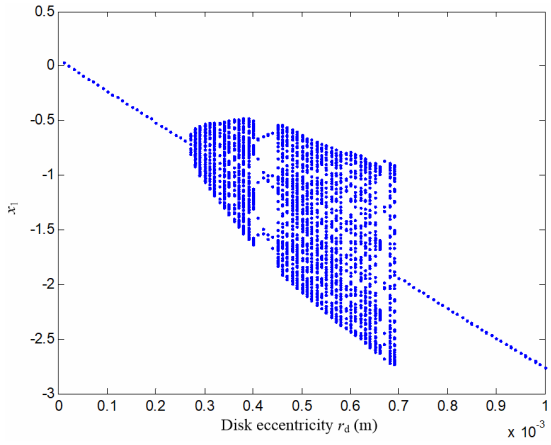

(a) Bifurcation diagram

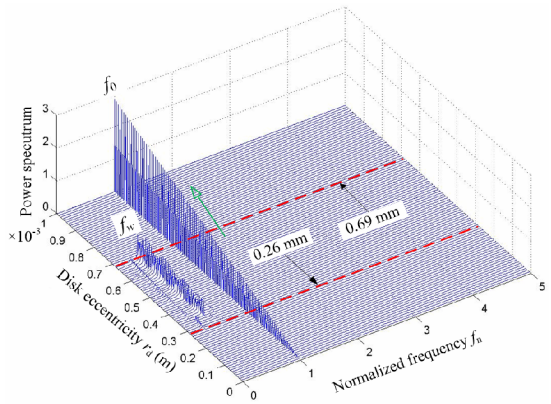

(b) Spectrum cascade

Fig. 8. Bifurcation diagram and spectrum cascade with varying disk eccentricity at ω = 1000 rad/s.

3.4 Effect of the disk mass

As the brush seal is a type of contact seal, the bristle pack would keep contact with the disk to guarantee the sealing effect. So the sealing performance largely depends on the disk

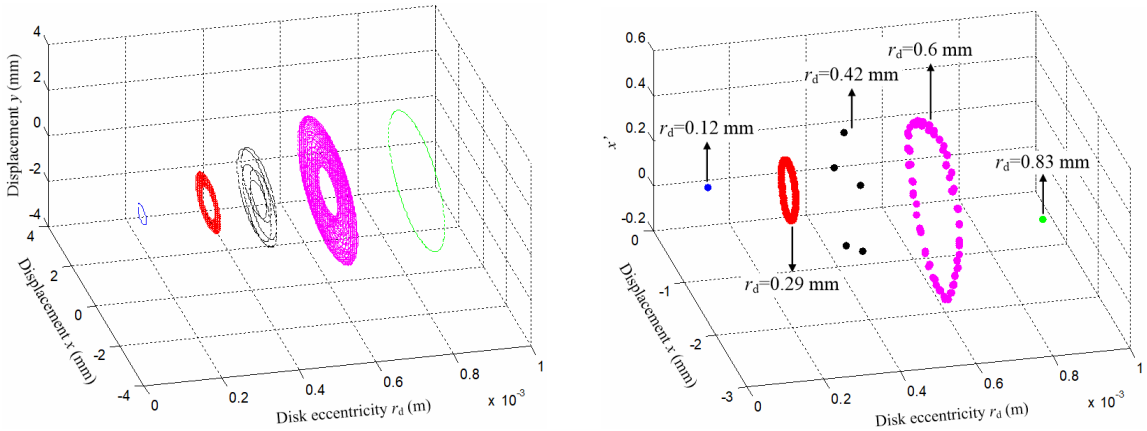

(a) Axis orbit (b) Poincaré map

Fig. 9. Vibration response with different dick eccentricity at ω = 1000 rad/s.

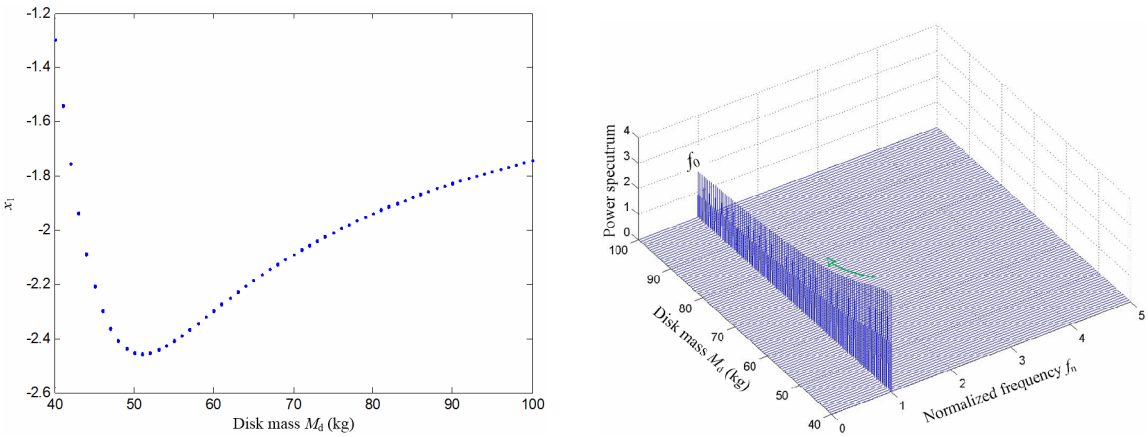

(a) Bifurcation diagram (b) Spectrum cascade

Fig. 10. Bifurcation diagram and spectrum cascade with varying disk mass at ω = 500 rad/s.

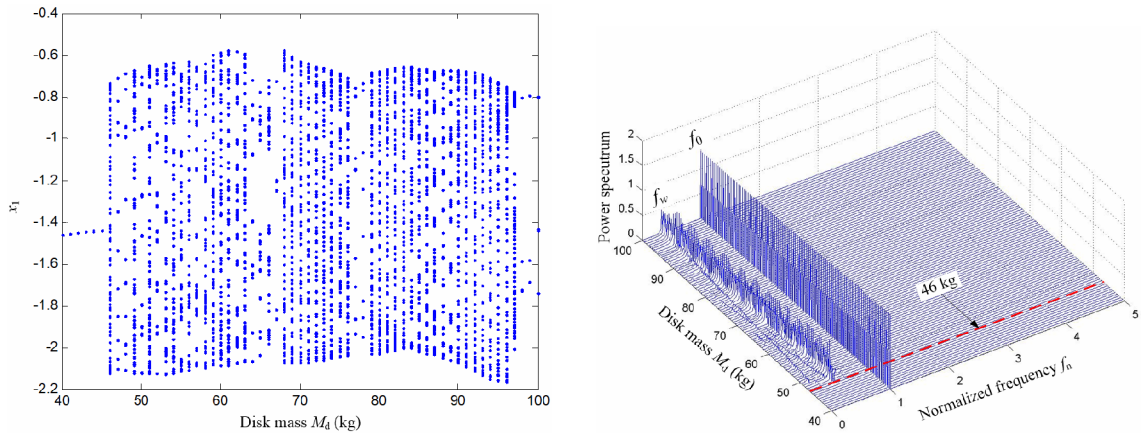

(a) Bifurcation diagram (b) Spectrum cascade

Fig. 11. Bifurcation diagram and spectrum cascade with varying disk mass at ω = 1000 rad/s.

mass. As observed in Fig. 10, the bifurcation diagram is a single line at ω = 500 rad/s , which represents the system is in period-1 motion. The vibration amplitude decreases with the increases of disc mass at first when M_d is less than 51 kg, then increases with disc mass when $M_d \geq 51$ kg. And there is only one frequency component f_0 dominating the spectrum cascade.

As plotted in Fig. 11, the system is in period-1 motion in lower disk mass range of $M_d \in [40,46]$ kg at $\omega = 1000$ rad/s . But the system is in quasi-periodic motion and period-n motion when $M_d \geq 46$ kg. The frequency component f_w is about

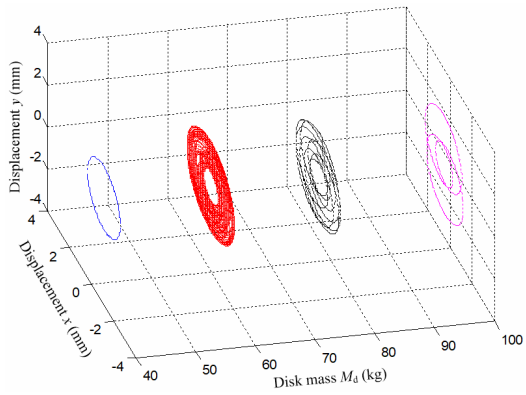

(a) Axis orbit

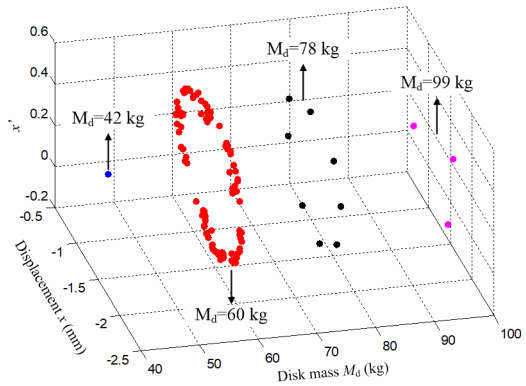

(b) Poincaré map

Fig. 12. Axis orbit and Poincaré map of the system at ω = 1000 rad/s.

half fundamental frequency components $0.5f_0$, and oil whip phenomena may arise at this time. It is obvious that the system stability is enhanced with smaller disk mass at $\omega = 1000$ rad/s. Axis orbit and Poincaré map in Fig. 12 represent that while disk mass is 60, 78, and 99 kg, the system is in quasi-periodic, period-8, and period-3 motion, respectively.

4. Conclusions

For the investigation of dynamic characteristics of a rotor-bearing-seal system, a nonlinear seal force with bristle radial interference is presented by adopting superposition method, and the short bearing theory is used to build the nonlinear oil-film force model. The effects of main parameters containing rotor rotational speed, installing interval, disc eccentricity, and disk mass on the dynamic behaviors of the rotor system are discussed. The conclusions from this study can be summarized:

(1) The vibration amplitude of the system with bristle interference is a bit larger than that without interference.

(2) The vibration amplitude of the system drops sharply at lower installing interval.

(3) When disc eccentricity is varying from 0 to 1 mm at $\omega = 500$ rad/s, bifurcation diagram branching at small disc eccentricity values undergoes period-n and quasi-periodic motion.

(4) The combination frequency components triggered by oil-film force and system stability are enhanced with smaller disk mass at a higher rotational speed.

Acknowledgments

This research is financially supported by National Natural Science Foundation of China (Grant Nos. 11802168 and 51575331).

Nomenclature

e : Eccentricity of rotor
E : Modulus of elasticity
F_{sx} : Seal force in the x direction
F_{sy} : Seal force in the y direction
h : Bristle radial interference
I : Moment of inertia of bristle
L_1 : Projection of the bristle AB on u axis
L_2 : Length of bearing
M_d : Disk mass
M_b : Bearing mass
M_q : Bending moment induced by distributed load of flow
M_F : Moment induced by contact force
O : Bearing geometric center
O_1 : Disk geometric center
O_2 : Journal geometric center
F_b : Contact force between the bristle and rotor
q_0 : Uniformly distributed load of fluid flow
r_d : Eccentricity of disc
R : Rotor radius
R_b : Distance between O_1 and the bottom of the front plate
s : Arc-length coordinate along the bristle
α : Angle of BO_1F
μ : Angle between O_1B and reverse extending line of F_b
ρ : Bristle radius of curvature
ω : Rotor rotational speed
δ : Installation spacing between the rotor surface and housing
Φ : Included angle between O_1A and y coordinate
φ : Bristle slope angle
θ : Bristle lay angle

References

[1] R. E. Chupp and P. Nelson, Evaluation of brush seals for limited-life engines, *J. of Propulsion and Power*, 9 (1) (1993) 113-119.

[2] J. F. Short, P. Basu, A. Datta, R. G. Loewenthal and R. J. Prior, Advanced brush seal development, *Proceedings of the 32nd AIAA/ASME/SAE/ASEE Joint Propulsion Conference and Exhibit*, Lake Buena Vista, FL, USA, July 1-3 (1996).

[3] F. E. Aslan-zada, V. A. Mammadov and F. Dohnal, Brush seals and labyrinth seals in gas turbine applications, *Proc.*

Instn Mech. Engrs Part A, J. of Power and Energy, 227 (2) (2013) 216-230.

[4] R. Flower, Brush seal development system, *Proceedings of the 26st AIAA/ASME/SAE/ASEE Joint Propulsion Conference and Exhibit*, Orlando, FL, USA, July 16-18 (1990).

[5] C. A. Long and Y. Marras, Contact force measurement under a brush seal, *International Gas Turbine and Aeroengine Congress and Exposition* (1995).

[6] M. C. Sharatchandra and D. L. Rhode, Computed effects of rotor-induced swirl on brush seal performance-part 2: Bristle force analysis, *J. of Tribology*, 118 (1996) 920-926.

[7] H. Zhao and R. J. Stango, Effect of flow-induced radial load on brush/rotor contact mechanics, *J. of Tribology*, 126 (1) (2004) 208-215.

[8] M. Demiroglum, M. Gursoy and J. A. Tichy, An investigation of tip force characteristics of brush seals, *Proceedings of ASME Turbo Expo 2007: Power for Land, Sea and Air,* Montreal, Canada, May 14-17 (2007).

[9] X. Shen, J. Jia, M. Zhao and J. Jing, Experimental and numerical analysis of nonlinear dynamics of rotor-bearing-seal system, *Nonlinear Dynamics*, 53 (2008) 31-44.

[10] H. Ma, H. Li, H. Niu, R. Song and B. Wen, Nonlinear dynamic analysis of a rotor-bearing-seal system under two loading conditions, *Journal of Sound and Vibration*, 332 (2013) 6128-6154.

[11] M. Zhang, J. Yang, W. Xu and Y. Xia, Leakage and rotordynamic performance of a mixed labyrinth seal compared with that of a staggered labyrinth seal, *Journal of Mechanical Science and Technology*, 31 (5) (2017) 2261-2277.

[12] Y. Wei and S. Liu, Nonlinear dynamics analysis of rotor-brush seal system, *Transactions of the Canadian Society for Mechanical Engineering*, 43 (2) (2019) 209-220.

[13] G. Capone, Analytical description of fluid-dynamic force field in cylindrical journal bearing, *L'Energia Elettrica*, 3 (1991) 105-110.

[14] G. Adiletta, A. R. Guido and C. Rossi, Chaotic motions of a rigid rotor in short journal bearings, *Nonlinear Dynamics*, 10 (3) (1996) 251-269.

[15] S. Xiao, S. Liu, F. Jiang, M. Song and S. Cheng, Nonlinear dynamic response of reciprocating compressor system with rub-impact fault caused by subsidence, *Journal of Vibration and Control*, 25 (11) (2019) 1737-1751.

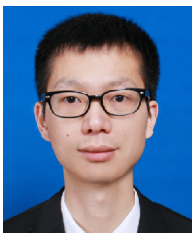

Yuan Wei received his Ph.D. from Harbin Institute of Technology, China, in 2017, and joined the School of Mechatronics Engineering and Automation, Shanghai University, Shanghai, China, in 2018. His research interests include rotor dynamics, nonlinear dynamics, vibration and control.

Shulin Liu received his Ph.D. from Harbin Institute of Technology, China, in 2003. He is a Professor of Mechatronic Engineering and Automation, Shanghai University, Shanghai, China. His research interests include nonlinear dynamics, fault diagnosis, vibration and control.